Earthquakes and Structures, *Vol. 13, No. 5 (2017) 443-454*
DOI: https://doi.org/10.12989/eas.2017.13.5.443

Performance-based seismic design of eccentrically braced steel frames using target drift and failure mode

Shen Li*, Jian-bo Tian[a] and Yun-he Liu[b]

School of Civil Engineering and architecture, Xi'an University of Technology, Xi'an Beilin District Jinhua Road No. 5, 710048, P. R. China

(Received April 11, 2017, Revised December 7, 2017, Accepted December 8, 2017)

Abstract. When eccentrically braced steel frames (EBFs) are in the desired failure mode, links yield at each layer and column bases appear plastically hinged. Traditional design methods cannot accurately predict the inelastic behavior of structures owing to the use of capacity-based design theory. This paper proposes the use of performance-based seismic design (PBSD) method for planning eccentrically braced frames. PBSD can predict and control inelastic deformation of structures by target drift and failure mode. In buildings designed via this process, all links dissipate energy in the rare event of an earthquake, while other members remain in elastic state, and as the story drift is uniform along the structure height, weak layers will be avoided. In this condition, eccentrically braced frames may be more easily rehabilitated after the effects of an earthquake. The effectiveness of the proposed method is illustrated through a sample case study of ten-story K-type EBFs and Y- type EBFs buildings, and is validated by pushover analysis and dynamic analysis. The ultimate state of frames designed by the proposed method will fail in the desired failure mode. That is, inelastic deformation of structure mainly occurs in links; each layer of links involved dissipates energy, and weak layers do not exist in the structure. The PBSD method can provide a reference for structural design of eccentrically braced steel frames.

Keywords: performance-based seismic design; eccentrically braced steel frames; failure mode; link; weak layer

1. Introduction

While steel moment frames can exhibit stable inelastic and ductile behavior under cyclic seismic excitation, concentrically braced frames usually possess greater lateral stiffness, which can limit the damage due to drift. However, moment frames are relatively flexible and drift limitations usually govern their design in order to control possible damage (Hjelmstad and Popov 1984). On the other hand, the ductility and energy dissipation capacity of concentrically braced frames can significantly deteriorate if braces buckle under seismic loading. Eccentrically braced frames (EBFs) successfully combine the advantages of moment frames and concentrically braced frames, namely, high ductility and lateral stiffness, while eliminating the shortcomings of those frames by limiting the inelastic activity to ductile shear links and keeping braces permanently elastic without buckling, thus maintaining high lateral stiffness during earthquake events. (Daneshmand and Hashemi 2012, Engelhardt and Popov 1992, Ashikov *et al.* 2016) Links act as a structural fuse that can dissipate seismic input energy without degradation of strength and stiffness. (Kasai and Popov 1986, Hjelmstad and Popov 1983, Berman and Bruneau 2007, Malley and Popov 1984). EBFs are easy to rehabilitate after an earthquake because of these replaceable links (Mansour *et al.* 2011, Shen *et al.* 2011). The length of links is based on structural height and span of EBFs, and its behavior with different brace patterns has been investigated (Bosco and Rossi 2009, Foutch 1989, Lian 2015, Wang 2016, Azad 2017). Configurations of typical EBFs are shown in Fig. 1.

EBFs with shear links have the excellent bearing capacity and stable energy dissipation; shear links are also recommended by design specification (AISC341-10). The links serve as the structural fuses, yielding under major earthquake and dissipating energy while the other frame components remain elastic. For this performance, current rules for the design of EBFs suggest that non-energy-dissipating members be designed by anticipating projected earthquake forces and multiplying by the magnification coefficient; as a result, the cross sections of columns and beams are oversized, which is difficult to apply in practical engineering (Speicher 2016).

Furthermore, the current seismic design method rules are capacity design based on elastic structural behavior with inelastic behavior only considered indirectly through certain modification factors. However, it is well known that structures designed according to current codes experience large inelastic deformations during major earthquakes; it is difficult to ensure the desired failure mode. A performance-based seismic design (PBSD) method of EBFs is proposed in this paper. The PBSD method can predict and control inelastic deformation of structures by target drift and failure mode, and weak layers can be avoided. In this study,

*Corresponding author, Lecturer
E-mail: lishen2861@163.com
[a]Lecturer
E-mail: tianjianbo2006@sina.com
[b]Professor
E-mail: liuyhe@xaut.edu.cn

ISSN: 2092-7614 (Print), 2092-7622 (Online)

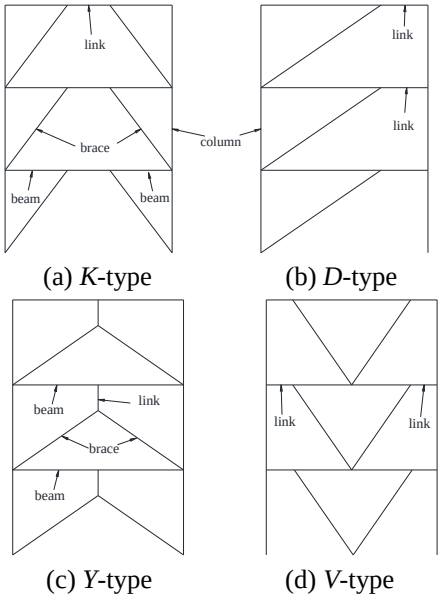

(a) *K*-type (b) *D*-type

(c) *Y*-type (d) *V*-type

Fig. 1 Types of EBFs

ten-story buildings with *K*-type EBFs and *Y*-type EBFs are designed by PBSD method. Two types of EBFs structures are tested by pushover analysis and dynamic analysis to demonstrate the superiority of the PBSD method.

2. Performance-based seismic design

The desired yielding mechanism in PBSD is links yielding to dissipate energy at each layer. Story drift is uniform along the structure height and other members still elastic when EBFs structure under rare earthquake. Finally, the column base appears plastically hinged. The performance-based seismic design method uses pre-selected target drift and failure modes as key performance objectives. This method has previously been successfully applied to steel and concrete moment-resisting frames (Lee *et al*. 1998, 2004, Liao 2010). The PBSD procedure is aimed at achieving predictable and controllable behaviour of structures during design level seismic events. Three major factors are essential in achieving this goal:

1) A design lateral force distribution that reflects realistic story shear distribution along the height of the structure when subjected to severe earthquakes. The triangular force distribution used in most design codes is derived from elastic analysis and may not be valid in the inelastic state. Therefore, a design lateral force distribution derived from nonlinear dynamic analysis results and calibrated by representative ground motion records is more appropriate for a performance-based design procedure.

2) A predictable global failure mode is highly desirable so that damage can be confined to pre-selected locations of the frame. In this regard, elastic design procedure cannot guarantee a predictable failure mechanism due to the predominantly inelastic nature of the structure's response during severe earthquakes. Therefore, plastic design procedure is more suitable for purposes of performance-based seismic design because a desirable yield mechanism

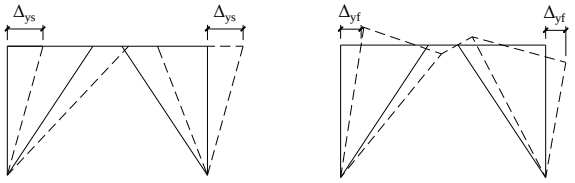

(a) shear component (b) bending component

Fig. 2 Yielding drift of eccentrically braced frame

is preselected. This design procedure was developed and successfully validated by Goel *et al*. through nonlinear dynamic analyses for steel moment resistant frames (Lee *et al*. 2004, 2012).

3) A pre-designated target drift limit that can be incorporated in determination of the design base shear. Story drift is a good design parameter to achieve target building performance objectives (such as immediate occupancy, collapse prevention, etc.) for selected earthquake hazard levels. Therefore, a design base shear based on selected target drift level, stiffness of the structure, ductility reduction factor, and structural ductility factor was used in this study. This design base shear was derived from modified energy balance equations and the proposed lateral force distribution (Chao *et al*. 2007).

2.1 Yield drift and target drift

Yield drift is one of the main parameters used in the PBSD method for calculation of the design base shear. The system target ductility demand will change with the yield drift. Therefore, having a good estimation of the yield drift is necessary in order to find the appropriate design base shear for a system that can meet the desired performance objectives. For different structures, the yield drift θ_y is variable. For regular MRFs, yield drift is approximately 1.0% regardless of their height or bay width. However, structural height and span have a large impact on the yield drift of EBFs. For instance, the yield drift of EBFs significantly increases with the increase in the height of the frame.

The yield drift θ_y of EBFs divide into shear drift θ_{ys} and bending drift θ_{yf}. For *K*-type EBFs, the shear component of deformation comes from axial deformation of the braces, and the flexural component is caused by axial deformation of the columns, as shown in Fig. 2.

For a one-story one-bay K-type EBFs (Fig. 2), the shear component of the yield drift can be obtained as, since $\tan\theta=h/a$, then

$$\Delta_{ys} = \varepsilon_y a\left(1+\tan^2\theta\right) = \frac{\varepsilon_y h\left(1+\tan^2\theta\right)}{\tan\theta} = \frac{2\varepsilon_{yb} h}{\sin 2\theta} \tag{1}$$

Therefore the shear component of the yield drift can be obtained as

$$\theta_{ys} = \frac{2 f_{yb}}{E \sin 2\theta} \tag{2}$$

where f_{yb} is yield strength of the braces, and E is the modulus of elasticity.

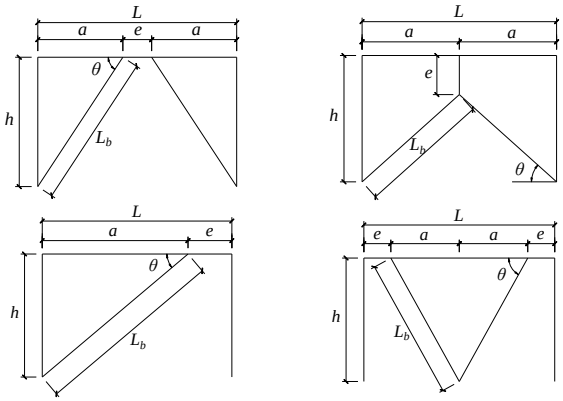

Fig. 3 Dimension of eccentrically braced frames

As can be seen from Eq. (2), the yield drift due to shear deformations only depends on the yield strength of the braces and the geometry parameter θ. For a regular EBF, the angle θ is almost the same in all stories. Hence, a largely equal story drift due to shear at the yield state can be expected for different stories in a multi-story EBFs.

The flexural component of the story drift at yield state for the one-story one-bay EBF shown in Fig. 3 can be obtained by considering the frame as a cantilever beam in which the two columns are acting as flanges in tension and compression. Then the flexural deformation of the frame can be calculated as follows

$$\sigma = \frac{Mc}{I} \tag{3}$$

where σ is the average axial stress in columns owing to the overturning moment, M, caused by the lateral loads. If the frame is assumed to behave like a beam, the moment of inertia, I can be estimated as

$$I = 2 \times A_c \times L^2 / 4 = \frac{A_c L^2}{2} \tag{4}$$

where A_c is the area of the column cross section and $c=L/2$. Therefore, the average strain in columns can be estimated as

$$\varepsilon = \frac{\sigma}{E} = \frac{M}{EA_c L} = \frac{FH}{EA_c L} \tag{5}$$

The vertical axial deformation of the columns can be obtained as

$$\Delta_{vert} = \int_0^H \varepsilon dy = \frac{FH^2}{EA_c L} \tag{6}$$

The horizontal drift due to this vertical deflection, which is basically the flexural component of the story drift, can be obtained as

$$\Delta_{horiz} = \Delta_{vert} \times \frac{H}{L} = \frac{FH^3}{EA_c L^2} \tag{7}$$

In order to obtain the horizontal deflection due to flexural mode of deformation at any level in a multi-story EBFs, the above approach can be followed. The vertical deflection can be calculated from Eq. (6) by assuming an approximately constant average axial strain in columns, ε_{avg}. This axial strain should be only due to the lateral loads. Then, the horizontal deflections can be found by multiplying vertical deflections by H/L.

$$\Delta_{horiz} = \Delta_{vert} \times \frac{H}{L} = \varepsilon_{avg} \times \frac{H^2}{L} \tag{8}$$

Thus, the flexural component of the yield drift can be estimated as

$$\theta_{\mathrm{yf}} = \varepsilon_{avg} \times \frac{H}{L} \tag{9}$$

As can be seen from the above equation, the yield drift caused by flexural deformation depends on the height of the frame and also the bay width. A reasonable estimate of the average axial strain in columns is needed for calculating yield drift. First, it is assumed that approximately 20% of the axial capacity of columns is utilized by the gravity loads. Then, assuming that the column sections are the same for every three stories, axial force design ratios of 0.9, 0.7, and 0.50 can be assumed at mechanism for these columns. In these estimations the bending moments in the columns are assumed to be negligible compared to the axial forces. Since these design ratios are under combined gravity and lateral loading, the ratios utilized only by lateral loads are 0.70, 0.50, and 0.30. Hence, the average axial stress in these three columns due to the lateral loads would be (0.70 + 0.50 +0.30)/3=0.50. The column axial stress capacity can be estimated as

$$\theta_{\mathrm{yf}} = \varepsilon_{avg} \times \frac{H}{L} = \frac{0.5 f_{\mathrm{yc}}}{E\gamma_{\mathrm{R}}} \cdot \frac{H}{L} \tag{10}$$

where f_{yc} is yield strength of the columns, and γ_R is the material partial coefficients. For Q235 (f_y=235 MPa) and Q345 (f_y=345 MPa) materials, γ_R is equal to 1.087 and 1.111 respectively.

Therefore, the yield drift of EBFs can be estimated as

$$\theta_{\mathrm{y}} = \theta_{\mathrm{ys}} + \theta_{\mathrm{yf}} = \frac{2 f_{\mathrm{yb}}}{E \sin 2\theta} + \frac{0.5 f_{\mathrm{yc}}}{E\gamma_{\mathrm{R}}} \cdot \frac{H}{L} \tag{11}$$

It is worth noting that a has different meanings. For K-type EBFs, a is equal to $(L-e)/2$. However, for D-type, V-type and Y-type EBFs, a is equal to $(L-e)$, $(L-2e)/2$ and $L/2$, respectively. Moreover, the L_b of Y-type EBFs differs from others; the length is related to $H-e$, and therefore, yield drift of Y-type EBFs can be estimated as

$$\theta_{\mathrm{y}} = \theta_{\mathrm{ys}} + \theta_{\mathrm{yf}} = \frac{2 f_{\mathrm{yb}}}{E \sin 2\theta} \frac{h-e}{h} + \frac{0.5 f_{\mathrm{yc}}}{E\gamma_{\mathrm{R}}} \cdot \frac{H}{L} \tag{12}$$

Ultimate drift is one of main parameters used in the PBSD method for calculation of the design ductility factor. Link plastic rotation angle (γ_p) can be easily estimated by frame geometry assuming the rigid-plastic behavior of the frame members. The relationship between plastic story drift angle (θ_p) and link plastic rotation angle (γ_p) for the four types of EBFs is shown in Fig. 4.

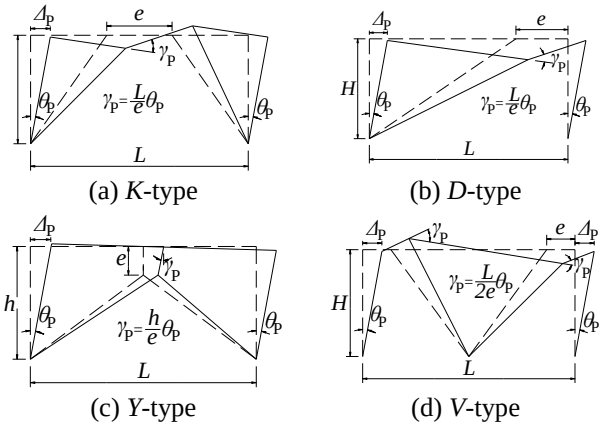

(a) *K*-type (b) *D*-type

(c) *Y*-type (d) *V*-type

Fig. 4 Link rotation angle for EBFs

For shear yielding links, the maximum value of link plastic rotation angle is 0.08 rad (AISC341-10), and that plastic story drift angle (θ_p) is equal to ultimate drift (θ_u) minus yield drift (θ_y). Therefore, the ultimate drift θ_u can be estimated as

For *K*-type and *D*-type EBFs:

$$\theta_{\mathrm{u}} = \gamma_{\mathrm{p}} \frac{e}{L} + \theta_{\mathrm{y}} = 0.08 \frac{e}{L} + \theta_{\mathrm{y}} \tag{13}$$

For *V*-type EBFs:

$$\theta_{\mathrm{u}} = \gamma_{\mathrm{p}} \frac{2e}{L} + \theta_{\mathrm{y}} = 0.16 \frac{e}{L} + \theta_{\mathrm{y}} \tag{14}$$

For *Y*-type EBFs:

$$\theta_{\mathrm{u}} = \gamma_{\mathrm{p}} \frac{e}{h} + \theta_{\mathrm{y}} = 0.08 \frac{e}{h} + \theta_{\mathrm{y}} \tag{15}$$

In the above equations, h is story height; H/L is the frame height to bay width.

2.2 Failure mode

EBFs subjected to design lateral forces and pushed to its maximum drift state are as shown in Fig. 5. All the inelastic deformations are intended to be confined within the shear links in the form of shear yielding. Since the plastic hinges developed at the column bases are almost inevitable in a major earthquake, the desired global failure mode of an EBF is formed by yielding (due to shear force) of the shear links plus the plastic hinges at the column bases. The gravity loads (dead load and live load) are assumed to be uniformly distributed, and no pattern loading is considered for live loads.

2.3 Design lateral forces

It is known that building structures designed according to current code procedures are expected to undergo large deformations in the inelastic range when subjected to major earthquakes. However, the equivalent static design lateral forces in the current codes are obtained from simplified models assuming that the structures behave elastically and

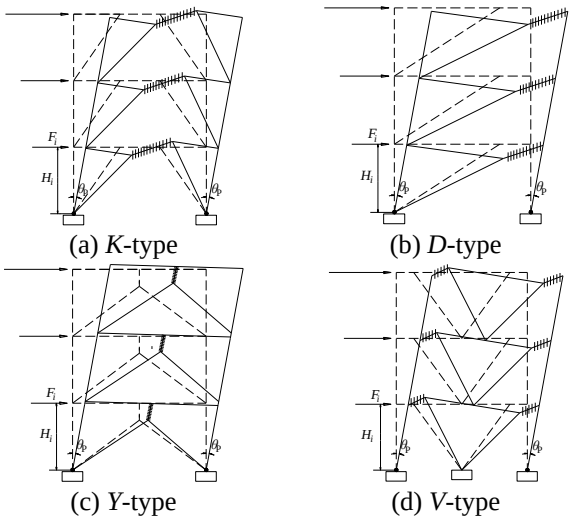

(a) *K*-type (b) *D*-type

(c) *Y*-type (d) *V*-type

Fig. 5 Failure mode of EBFs

primarily in the first mode of vibration. Thus, during earthquakes, this leads such structures to experience lateral force distributions considerably different from those assumed by the code formulas. In order to achieve the main goal of performance-based seismic design, i.e., a desirable and predictable structural response, it is necessary to account for inelastic behavior of structures directly in the design process. The commonly used elastic analysis and design procedures in current practice, along with elastic design lateral force distributions, do not fulfill this goal in a realistic manner.

Unlike the force distribution in the current codes, the design lateral force distribution used in the PBSD method is based on maximum story shears as observed in nonlinear time-history analysis results. This new design lateral force distribution has been found suitable for MF, EBF, CBF, and STMF. Analytical results have shown that:

1) Frames designed by using this lateral force distribution experienced more uniform maximum interstory drifts along their height than the frames designed by using current code distributions;

2) This force distribution also provides a perfect estimate of maximum column moment demands when the structures are responding to severe ground motions and deform into the inelastic range;

3) Higher mode effects are well reflected in the proposed design lateral force distribution. This lateral force distribution is expressed as follow.

$$\beta_i = \frac{V_i}{V_{\mathrm{n}}} = \left(\frac{\sum_{j=i}^{n} G_j H_j}{G_{\mathrm{n}} H_{\mathrm{n}}} \right)^{0.75T^{-0.2}} \tag{16}$$

when $i=n$, $\beta_{n+1}=0$

where $F_n = V \left(\dfrac{G_n H_n}{\sum_{j=1}^{n} G_j H_j} \right)^{0.75T^{-0.2}}$

In the above equations, β_i represents the shear distribution factor at level *i*; V_i and V_n , respectively, are the story shear forces at level *i* and at the top (*n*th) level; G_j is the seismic weight at level *j*; H_j is the height of level *j* from the base; G_n is the weight at the top level; H_n is the height of roof level from base; T is the fundamental period; F_i is the lateral force at level *i*; and V is the total design base shear.

2.4 Design base shear

Calculation of the required design base shear is one of the main steps in the PBSD procedure. The design base shear in this method is derived based on the inelastic state of the structure, with the drift control built-in. Therefore, no separate drift check is needed after design. In this approach, the design base shear is determined by pushing the structure monotonically up to a target drift after the formation of a pre-selected failure mode. Note that no actual pushover analysis is needed for this as will be seen later. The amount of work needed is assumed as a factor γ times the elastic input energy for an equivalent EP-SDOF system (Housner 1956, 1960). It should be noted that the work mentioned above assumes no relationship with the actual energy dissipated during earthquake excitation, which has been used in energy-based procedures as proposed by many investigators (Akiyama 1985, Uang and Bertero 1988). However, those procedures have been found to be extremely cumbersome to implement in common design practice. In the PBSD method the needed work term (E_e+E_p) is simply used as a means to calculate the required design base shear by establishing ties between the desired failure mode, design drift, force-displacement characteristics of the structure and elastic input energy from the design ground motion.

Thus, the work-energy equation can be written as

$$E_{\mathrm{e}} + E_{\mathrm{p}} = \gamma\left(\frac{1}{2}MS_v^2\right) = \frac{1}{2}\gamma M\left(\frac{T}{2\pi}S_{\mathrm{a}}g\right)^2 \tag{17}$$

where E_e and E_p are, respectively, the elastic and plastic components of the energy (work) needed to push the structure up to the target drift. S_v is the design spectral pseudo velocity; and M is the total mass of the system. The energy modification factor, γ, depends on the structural ductility factor (μ_s) and the ductility reduction factor (R_μ).

Fig. 6 shows the relationship between the base shear (V) and the corresponding drift (Δ) of the elastic and corresponding elastic-plastic SDOF systems.

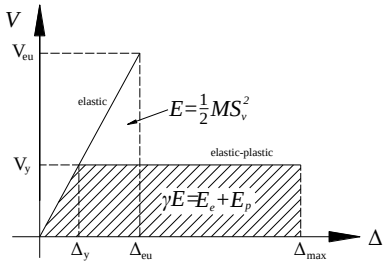

Fig. 6 Structural idealized response and energy balance concept for SDOF

Using the geometric relationship between the two areas representing work and energy in Fig. 6, Eq. (17) can be written as

$$\frac{1}{2}V_{\mathrm{y}}\left(2\Delta_{\max} - \Delta_{\mathrm{y}}\right) = \gamma\left(\frac{1}{2}V_{eu}\Delta_{eu}\right) \tag{18}$$

Eq. (18) can be reduced into the following form

$$\gamma\frac{\Delta_{eu}}{\Delta_{\mathrm{y}}} = \frac{\left(2\Delta_{\max} - \Delta_{\mathrm{y}}\right)}{\Delta_{eu}} \tag{19}$$

where Δ_{eu} and $\Delta_{\max}$ in Fig. 6 are equal to $R_\mu\Delta_y$ and $\mu_s\,\Delta_y$, respectively. Substituting these terms into Eq. (19), the expression for energy modification factor γ can be written as

$$\gamma = \frac{2\mu_{\mathrm{s}} - 1}{R_{\mu}^2} \tag{20}$$

where μ_s is the ductility factor equal to the design target drift divided by the yield drift ($\Delta_{\max}/\Delta_y$); R_μ is the ductility reduction factor equal to V_{eu}/V_y. It can be seen from Eq. (20) that the energy modification factor γ is a function of the ductility reduction factor (R_μ) and the ductility factor (μ_s). The method by (Newmark and Hall 1982) is used herein to relate the ductility reduction factor and the structural ductility factor for EP-SDOF as shown in Table 1 (Lee *et al.* 2012, Miranda and Bertero 1994). Plots of energy modification factor γ as obtained from Eq. (20).

Akiyama (1985) and other researchers have shown that the elastic vibrational energy, E_e, can be calculated by assuming that the entire structure can be reduced into an SDOF system, i.e.

$$E_{\mathrm{e}} = \frac{1}{2}M\left(\frac{T}{2\pi}\frac{V}{G}g\right)^2 \tag{21}$$

where V is the desired base shear at yield and G is the total seismic weight of the structure (G=Mg). Substituting Eq. (21) into Eq. (17) and rearranging the terms gives

$$E_{\mathrm{p}} = \frac{GT^2\mathrm{g}}{8\pi^2}\left(\gamma S_{\mathrm{a}}^2 - \left(\frac{V}{G}\right)^2\right) \tag{22}$$

Table 1 Ductility reduction factor R_μ and its corresponding structural period range

Period Range	Ductility Reduction Factor R_μ
$0 \le T < \frac{T_0}{10}$	$R_{\mu} = 1$
$\frac{T_0}{10} \le T < \frac{T_0}{4}$	$R_{\mu} = \sqrt{2\mu_{\mathrm{S}} - 1}\left(\frac{T_1}{4T}\right)^{2.513\log\left(\frac{1}{\sqrt{2\mu_{\mathrm{S}}-1}}\right)}$
$\frac{T_0}{4} \le T < T_0^{'}$	$R_{\mu} = \sqrt{2\mu_{\mathrm{S}} - 1}$
$T_0^{'} \le T < T_0$	$R_{\mu} = \frac{T}{T_0}\mu_{\mathrm{S}}$
$T_0 \le T$	$R_{\mu} = \mu_{\mathrm{S}}$

Note: T_0=0.57s, $T_0^{'} = T_0\frac{\sqrt{2\mu_{\mathrm{S}} - 1}}{\mu_{\mathrm{S}}}$

By using a pre-selected failure mode for a given structural system, as shown in Fig. 5, and equating the plastic energy term E_p to the external work done by the design lateral forces gives

$$E_{\mathrm{p}} = \sum_{i=1}^{n} F_i H_i \theta_{\mathrm{p}} \tag{23}$$

where θ_p is the global inelastic drift ratio of the structure (see Fig. 5), which is the difference between the pre-selected design drift ratio (θ_u) and yield drift ratio (θ_y).

Substituting Eqs (16) and (23) into Eq. (22), and solving for *V*/*G* gives

$$\frac{V}{G} = \frac{-\xi + \sqrt{\xi^2 + 4\gamma S_{\mathrm{a}}^2}}{2} \tag{24}$$

where V is the design base shear and ξ is a dimensionless parameter, which depends on the stiffness of the structure, modal properties, and design plastic drift level, and is given by

$$\xi = \left(\sum_{i=1}^{n} (\beta_i - \beta_{i+1}) H_i\right) \left(\frac{G_{\mathrm{n}} H_{\mathrm{n}}}{\sum_{j=1}^{n} G_j H_j}\right)^{0.75T^{-0.2}} \cdot \left(\frac{\theta_{\mathrm{p}} 8\pi^2}{T^2 g}\right) \tag{25}$$

It should be noted that the required design base shear given by Eq. (24) is related to the lateral force distribution (modal properties), design plastic drift ratio, and selected yield mechanism. Also note that in Eq. (25), β_{n+1}=0, when i=n.

3. Member design

3.1 Design of shear links

EBFs structure is pushed to target drift with desired failure mode, which is one objective of the PBSD method. For EBFs, designs of links as a key procedure in the PBSD method, because of plastic deformations, are isolated to links and column bases. In conditions where the distribution lateral force is known, yield shear links are proportioned to create uniform story drift along the structure height. For one bay by one frame EBFs, by using the principle of virtual work and equating the external work to the internal work, the following equation can be obtained

$$\sum_{i=1}^{n} F_i H_i \theta_{\mathrm{p}} + \frac{1}{2} \sum_{i=1}^{n} \omega_i L \theta_p (L - e) = 2M_{\mathrm{pc}} \theta_{\mathrm{p}} + \sum_{i=1}^{n} \beta_i V_{\mathrm{pr}} e \gamma_{\mathrm{p}} \tag{26}$$

where L is the span length, e is the length of shear link, ω_i is the vertical force in ith story beams, M_{pc} is the plastic moment of column base, V_{pr} is plastic shear strength of top story link, and $\beta_i V_{pr}$ is the plastic shear strength of ith story link.

As can be seen from the left hand side of equation, the first item is lateral force work, and the second item is vertical force work For *K*-type, *Y*-type and *V*-type EBFs, the vertical work is equal to zero due to anti-symmetric deformation occurring in the beams.

Fig. 4 shows the relationship between plastic rotation γ_p of links and plastic story drift θ_p of EBFs. In Eq. (26), θ_p instead of γ_p, equation can be written as

For *K*-type and *V*-type EBFs:

$$\beta_i V_{\mathrm{pr}} = \beta_i \frac{\left(\sum_{i=1}^{n} F_i H_i - 2M_{\mathrm{pc}}\right)}{L \sum_{i=1}^{n} \beta_i} \tag{27}$$

For D-type EBFs:

$$\beta_i V_{\mathrm{pr}} = \beta_i \frac{\left(\sum_{i=1}^{n} F_i H_i + \frac{1}{2} \sum_{i=1}^{n} \omega_i L \theta_p (L - e) - 2M_{\mathrm{pc}}\right)}{L \sum_{i=1}^{n} \beta_i} \tag{28}$$

For Y-type EBFs:

$$\beta_i V_{\mathrm{pr}} = \beta_i \frac{\left(\sum_{i=1}^{n} F_i H_i - 2M_{\mathrm{pc}}\right)}{\sum_{i=1}^{n} \beta_i h_i} \tag{29}$$

In order to design sections of shear links, the shearing strength of links must meet the requirements of the following equation:

$$\psi V_{\mathrm{p},i} = \psi \left(0.58 f_{\mathrm{y}} A_{\mathrm{w},i}\right) \geq \beta_i V_{\mathrm{pr}} \tag{30}$$

where ψ is strength reduction factor, ψ=0.9. f_y is the yielding strength of links and $A_{w,i}$ is the web area of ith story link.

3.2 Design of members outside the links

In order to avoid a weak layer in first floor, as shown in Fig. 7, the plastic moment of column base needs to meet the requirements

$$M_{\mathrm{pc}} = \frac{1.5 V' h_1}{4} \tag{31}$$

where V' is one-bay base shear, h_1 is the bottom story height and the factor 1.5 includes four components: design resistance factor(1/0.9), material over strength factor (1.1), safety factor(1.1) and stress ratio (1/0.9).

The relationship between axial force of brace and ultimate shear capacity of link can be estimated as follows

$$P_{\mathrm{brace}} = \frac{V_{\mathrm{u}}}{2\cos\theta} \tag{32}$$

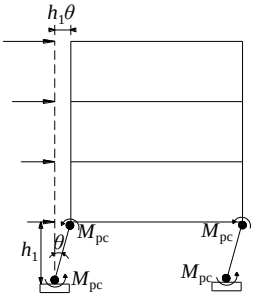

Fig. 7 One-bay frame with weak layer mechanism

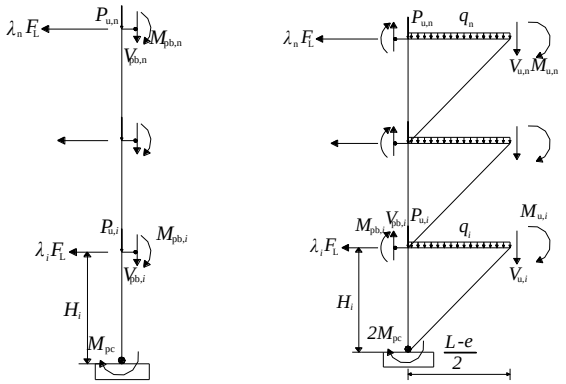

(a) Exterior column tree (b) Interior column tree

Fig. 8 Free body diagram of non-yielding members

where V_u is ultimate shear capacity of link.

The other members, namely, columns and beams outside of links, can be designed by free bodies. Fig. 8 shows *K*-type EBFs as an example.

In Fig. 8(a) shows the columns with no brace and (b) shows the column with braces. $V_{u,i}$ is the ultimate shear capacity of link at *i*th story, and the corresponding end moment of link is $M_{u,i}$. $M_{pb,i}$ is the plastic moment of beams with no braces, and the corresponding shear force is $V_{pb,i}$. M_{pc} is the plastic moment of column base. λ_i is the lateral force distribution coefficient, expressed as follows

$$\lambda_i = \frac{F_i}{\sum_{i=1}^{n} F_i} = \frac{(\beta_i - \beta_{i+1})}{\sum_{i=1}^{n} (\beta_i - \beta_{i+1})} \tag{33}$$

After yielding member is designed, the variables $V_{u,I}$, $M_{u,I}$, $M_{pb,i}$ and $V_{pb,i}$ are known. Take these forces as external forces to free bodies, and according to the force equilibrium condition, the lateral forces acting on the free bodies can be calculated.

The free bodies as shown in Fig. 8 can be buildings in an elastic structural analysis program. Take q_i, $\lambda_i F$, $V_{u,I}$, $M_{u,I}$, $P_{u,i}$ as external forces to free bodies, and the internal forces of braces, columns and beams outside the link can be calculated. Therefore, according to elastic design method currently used, the required sections of braces and columns can be designed.

4. Design procedure

The above introduced performance-based seismic design of eccentrically braced frames in detail. The PBSD method includes two segments: one is determining the essential parameters of the structure, the other one is member design, including yielding members and non-yielding members. The flow charts of the PBSD method are shown in Fig. 9 and Fig. 10.

5. Design examples

5.1 Design conditions

The design examples are characterized by the peak ground acceleration of 0.3 g with 10% probability of exceedance in a 50-year period and moderately firm ground conditions. The factor that reduces the elastic response

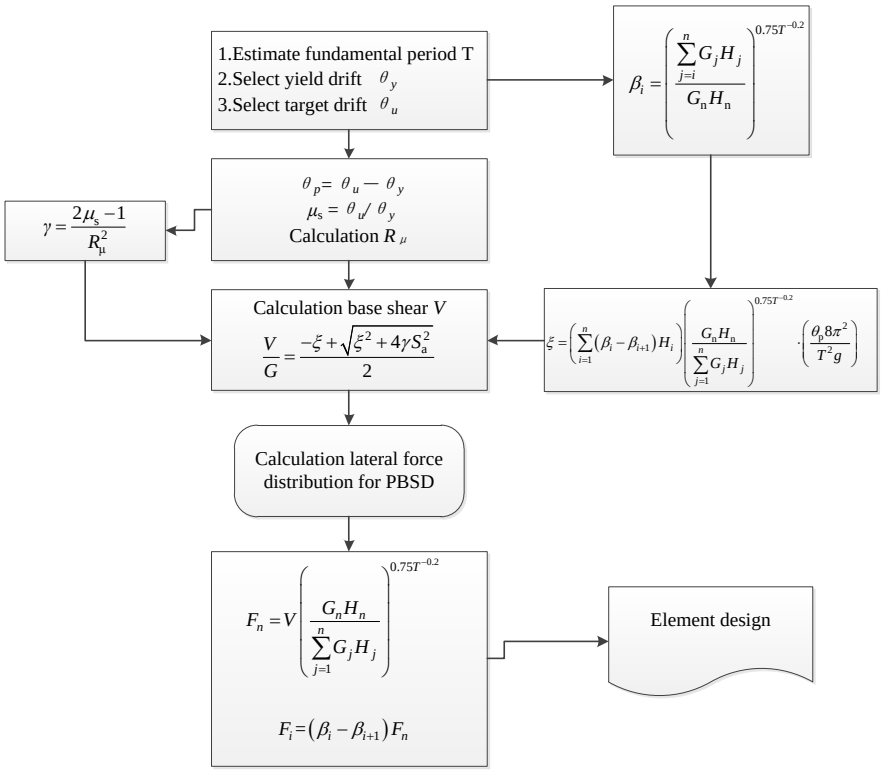

Fig. 9 Performance-based plastic design flowchart: design base shear and lateral force distribution

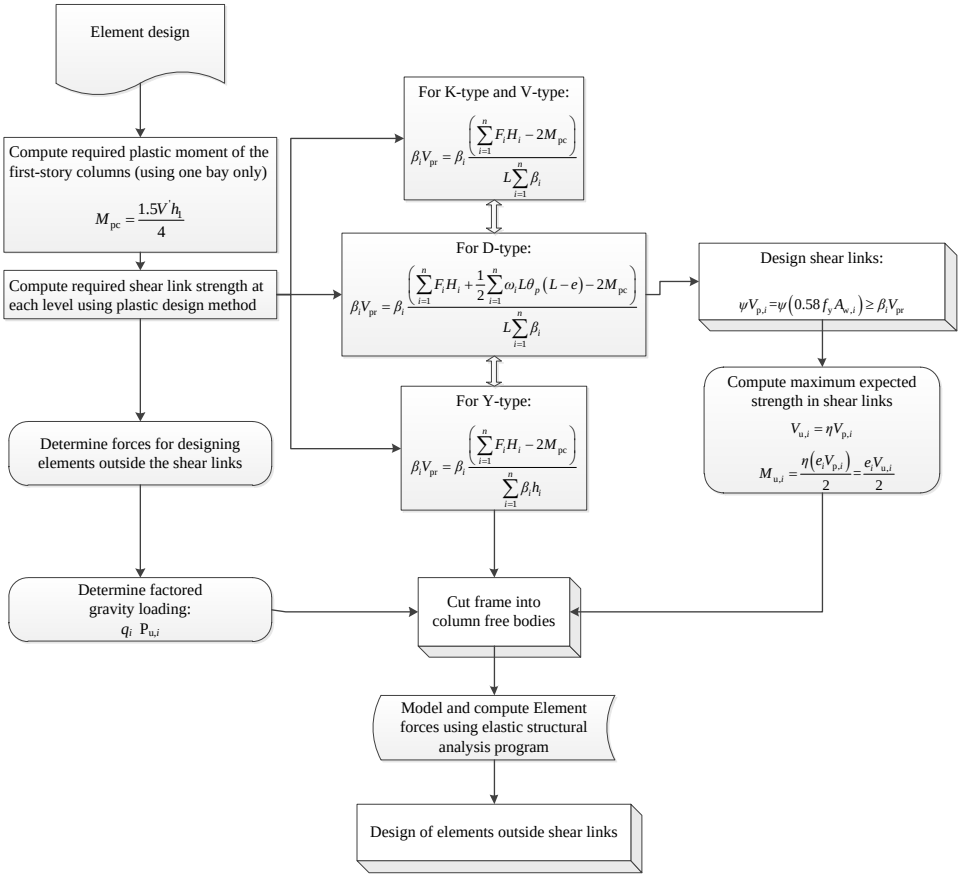

Fig. 10 Performance-based plastic design flowchart for EBF: element design

spectrum to obtain the design spectrum is 2.8125 in GB50011-2010. The Alpha damping α and Beta damping β were specified according to the damping ζ and the fundamental period of the structures. Moreover, damping of 4% is considered appropriate for a steel building with a structural height not exceeding 50 m, and 3% for structural heights between 50 and 200 m according to the requirements of GB50011-2010. In all design examples, the story height is 3.6 m; there are five bays in the *X*-direction and three bays in the *Y*-direction. The span in both *X*- and *Y*-directions is 7.2 m (see Fig. 11). The length of links for *K*-type EBFs and *Y*-type EBFs are 900 mm and 800 mm, respectively. The constraints between columns of different stories were continuous and rigid connections were used between columns and beams in all design examples. Furthermore, the link had the same section of the beam connected at the same story for *K*-type EBFs. The frames located along the perimeter were designed to resist seismic loads and incorporated eccentric braces in the central span (see Fig. 11). The dead load for the floors and roofs are, respectively, 4.5 kN/m^2 and 5.5 kN/m^2. The floor live load, roof live load, and snow load are 2, 0.5, and 0.25 kN/m^2, respectively. The detailed member sections are listed in Tables 2-3, in which 'H' refers to the welded H-shaped section. The H-section's accompanying numbers are section depth *h*, flange width b_f, web thickness t_w, and flange thickness t_f, respectively. '*B*' refers to the box section and the accompanying numbers are section depth *h*, section width *b* and wall thickness *t*, respectively, with unit of mm.

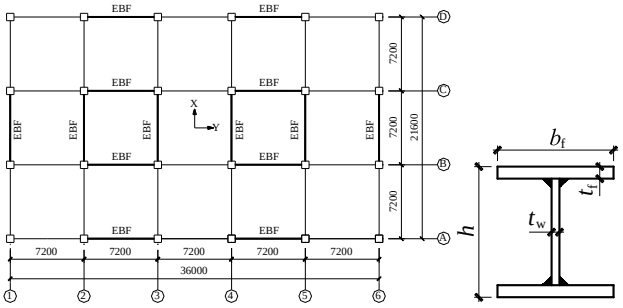

Fig. 11 Building plan view

5.2 Member sections

Member sections of the *K*-type and *Y*-type EBFs are designed based on the PBSD method, which list in Tables 2-3.

In order to investigate the behaviour of the sample buildings under major earthquakes, nonlinear analyses including both static pushover analysis and time-history dynamic analysis were conducted to compare the behaviour of the *K*-EBFs frames and the *Y*-EBFs frames. The analyses were performed using the SAP2000 program, which has a built-in shear link model.

5.3 Pushover analysis

A load combination of 1.2 (Dead Load)+0.5 (Live Load) was applied to the structures during nonlinear static

Table 2 Member sections of *K*-type eccentrically braced frame

Layer	Beams	Links	Interior Columns	Exterior Columns	Braces
10	H360×170 ×6×12	H330×160 ×6×12	B400× 400×16	B400× 400×16	H220×220 ×10×16
9	H410×200 ×10×16	H360×180 ×10×16	B450× 450×16	B450× 450×16	H220×220 ×10×16
8	H520×200 ×10×16	H470×180 ×10×16	B500× 500×18	B500× 500×18	H240×240 ×12×18
7	H550×200 ×12×18	H480×200 ×12×18	B500× 500×18	B500× 500×18	H240×240 ×12×18
6	H550×240 ×12×18	H540×200 ×12×18	B600× 600×18	B600× 600×18	H260×260 ×12×18
5	H550×240 ×14×20	H520×240 ×14×20	B600× 600×18	B600× 600×18	H280×280 ×12×18
4	H580×240 ×14×20	H560×240 ×14×20	B670× 670×22	B670× 670×22	H280×280 ×12×18
3	H600×240 ×14×20	H590×240 ×14×20	B670× 670×22	B670× 670×22	H280×280 ×12×18
2	H610×240 ×14×20	H600×240 ×14×20	B750× 750×24	B750× 750×24	H280×280 ×12×18
1	H620×240 ×14×20	H610×240 ×14×20	B750× 750×24	B750× 750×24	H280×280 ×12×18

Table 3 Member sections of *Y*-type eccentrically braced frame

Layer	Beams	Links	Interior Columns	Exterior Columns	Braces
10	H440×160 ×6×10	H320×140 ×5×10	B350× 350×16	B350× 350×12	H200×200 ×10×16
9	H480×200 ×8×12	H310×150 ×8×14	B400× 400×16	B350× 350×12	H200×200 ×10×16
8	H490×200 ×10×16	H430×180 ×8×14	B450× 450×18	B400× 400×16	H220×220 ×10×16
7	H530×220 ×10×16	H420×200 ×10×16	B450× 450×20	B400× 400×16	H220×220 ×10×16
6	H560×240 ×10×16	H470×200 ×10×16	B500× 500×20	B450× 450×18	H220×220 ×10×16
5	H540×240 ×12×18	H510×200 ×10×16	B500× 500×20	B450× 450×18	H250×250 ×10×16
4	H570×240 ×12×18	H470×200 ×12×18	B550× 550×22	B500× 500×20	H250×250 ×10×16
3	H590×240 ×12×18	H490×200 ×12×18	B550× 550×22	B500× 500×20	H250×250 ×10×16
2	H610×240 ×12×18	H510×200 ×12×18	B600× 600×25	B550× 550×20	H250×250 ×10×16
1	H620×240 ×12×18	H520×200 ×12×18	B600× 600×25	B550× 550×20	H250×250 ×10×16

pushover and time-history dynamic analyses. Both $P-\Delta$ and $P-\delta$ effects were accounted for in the analysis. The roof displacement was controlled via lateral force model using inverted triangle distributed load in the pushover analysis.

The pushover curves of *K*-type EBFs and *Y*-type EBFs are shown in Fig. 12. The *Y*- coordinates and *X*-coordinates are frame base shear and frame roof drift, respectively. The frame roof drift define as D/H, where D is the lateral displacement and H is the structure height. The lateral stiffness of *K*-EBFs is approximate with *Y*-EBFs, and the carrying capacity of *K*-EBFs is higher than *Y*-EBFs. However the ductility of *Y*-EBFs is better than *K*-EBFs, due to the links of *Y*-EBFs that are outside of the frames, thus

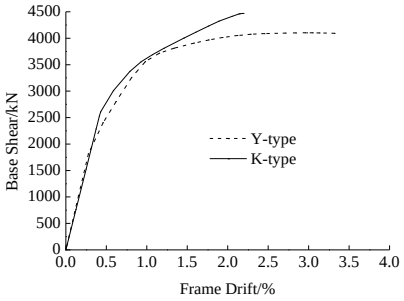

Fig. 12 Pushover curves

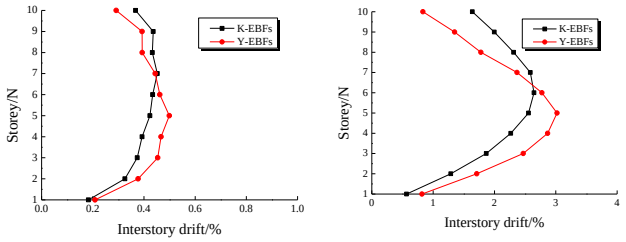

(a) Frame drift at 0.4% (b) Frame drift at 5%

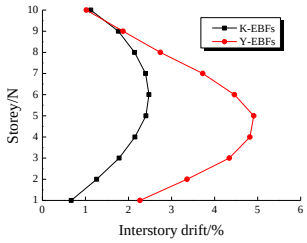

(c) ultimate state

Fig. 13 Interstory drift

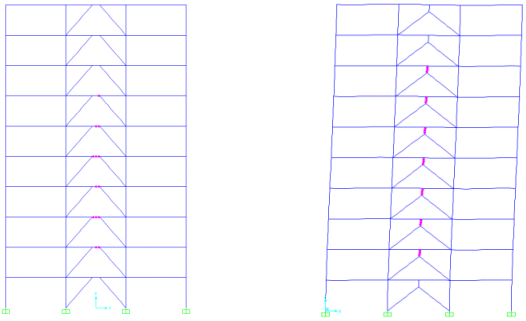

Fig. 14 Yield mechanism at 0.4% frame drift

the structure deformation is similar to moment-resisting frames. The yield mechanism of frames at roof drift 0.4% and 2% are shown in Figs. 14-15, respectively. The failure modes of frames in ultimate state are shown in Fig. 16. The elastic and inelastic code limitations of the structure are 0.4% and 2%, respectively. The ultimate state corresponds to the end of the pushover curves. In the elastic limitation, frame drift use roof drift instead of story drift, and the same is also used in inelastic limitation and ultimate state. The frame drift at 0.4% shows that only links produce inelastic deformation to dissipate energy, and the frame drift at 2% shows that, except all links that participate in energy dissipation, beams are the second line of defence by bending into plastic deformation. In the ultimate state, column bases become plastically hinged by *P-M* interaction.

Table 4 Ground motion records

No.	Earthquake number	Earthquake event	Station	Record/Component	*M*	*R*/km	*PGA*/g	*PGV*/(cm/s)
1	P0006	Imperial Valley	117 El Centro Array #9	IMPVALL/I-ELC180	7.0	8.3	0.313	29.8
2	P0016	Kern County	1095 Taft Lincoln School	KERN/TAF021	7.4	41.0	0.156	15.3
3	P1461	Chi-Chi, Taiwan	TCU095	ChiChi/TCU095-W	7.6	43.4	0.379	62.0
4	P0883	Northridge	24278 Castaic - Old Ridge Route	NORTHR/ORR090	6.7	20.1	0.568	52.1
5	P0126	Friuli, Italy	8012 Tolmezzo	FRIULI/A-TMZ270	6.5	15.5	0.315	30.8
6	P0764	Loma Prieta	47006 Gilroy - Gavilan Coll	LOMAP/GIL067	6.9	10.0	0.357	28.6
7	P0810	Cape Mendocino	89324 Rio Dell Overpass - FF	CAPEMEND/RIO360	7.0	14.3	0.549	42.1
8	P0816	Landers	22170 Joshua Tree	LANDERS/JOS000	7.3	11.0	0.274	27.5
9	P1043	Kobe Japan	0 KJMA	KOBE/KJM090	6.9	1.0	0.599	74.3
10	P0729	Superstitn Hills	01335 El Centro Imp. Co. Cent	SUPERST/B-SUP135	6.5	5.6	0.894	42.2

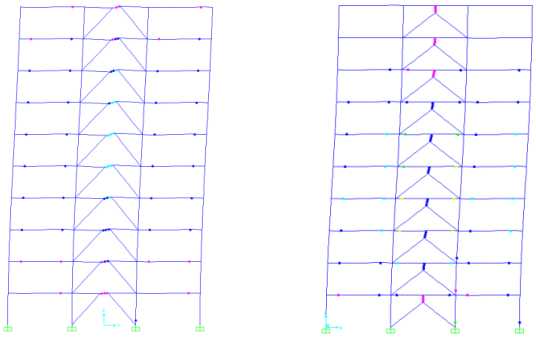

Fig. 15 Yield mechanism at 2% frame drift

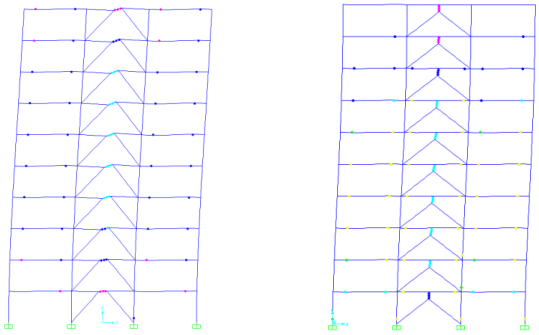

Fig. 16 Failure mode at ultimate state

5.4 Nonlinear time history analysis

In the nonlinear dynamic analysis, it is usual practice to use some viscous damping to account for the energy dissipation in addition to hysteretic energy. In this study, a critical viscous damping value of 5% was assumed. Ten 2% in 50 years (return period 1600 years to 2400 years) ground motions records from PEER ground motions database (http://peer.berkeley.edu/) were selected for the nonlinear time history analysis as shown in Table 4. *M* is earthquake magnitude (measured on the Richter scale), *R* is latest distance of the fault, *PGA* is maximum acceleration, and *PGV* is the maximum accelerated velocity. The spectra of the selected ground motions compared with the design spectra is shown in Fig. 17.

Owing to the limitation of Papers, two failure modes of

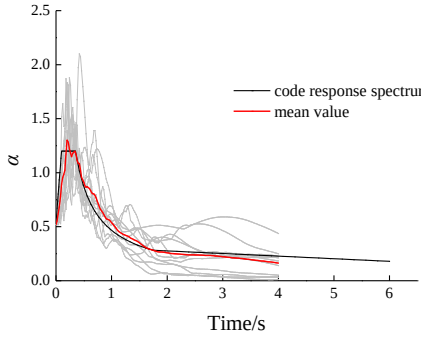

Fig. 17 Comparison between the design spectra and the spectra of the selected ground motions

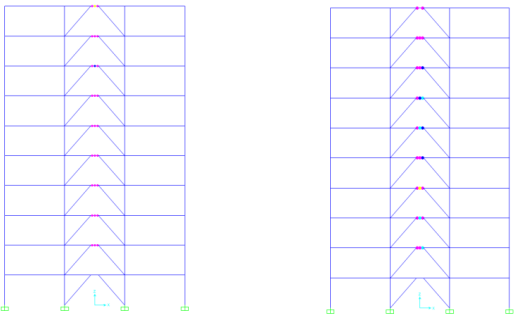

(a) P0006 (b) P0016

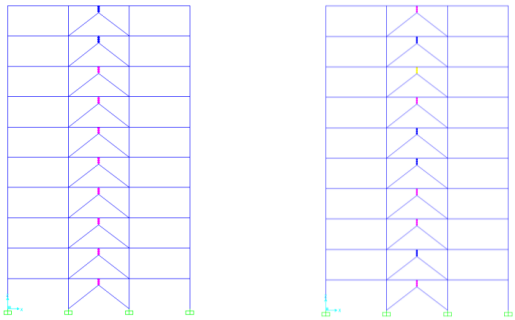

(c) P0006 (d) P0016

Fig. 18 Failure mode

K-type and *Y*-type EBFs during rare earthquakes are shown in Fig. 18. During severe earthquakes, for *K*-type and *Y*-type EBFs, the inelastic deformations are isolated in

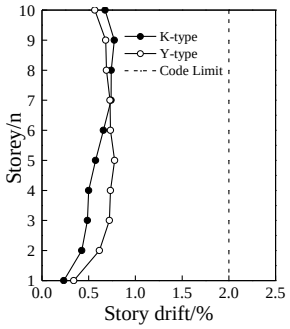

Fig. 19 Story drift

links, while other elements are still elastic. Moreover, all links participate in dissipating energy, and the failure modes of structures are almost close to the desired yield mechanism. The sample structure is designed by PBSD method. The mean values of story drift distribution along the structure height under severe earthquakes are as shown in Fig. 19. The ranges of story drift are within 0.45%-0.78% except for the first story; the story drifts of the first story are 0.23% and 0.34%, respectively. For *K*-type EBFs and *Y*-type EBFs, one reason for this change is that the lateral stiffness of the first story is higher than that of others; another is to avoid a weak layer in the first floor according to Eq. (31).

6. Conclusions

Yield drift and ultimate drift of EBFs are proposed as critical parameters for performance-based seismic design. Overall, the EBFs designed by the proposed method can be expected with reasonable confidence to satisfy the target performance objectives when subjected to a major earthquake, and need no further assessment after the first design. This is because the performance objectives, regarding the yield mechanism and maximum drift, are explicitly built into the determination of design lateral forces and design of the frame members. All the inelastic activity was confined to the shear links and the column bases in EBFs as intended. The story drift distribution along the structure height is uniform under rare earthquakes. The maximum inter-story drifts in the EBFs were within the 2% pre-selected target drift for all the selected 10% in 50 years ground motions. The proposed design procedure can control the seismic performance of the deformation-sensitive components, and the first inter-story drift is minimal because of the base stiffness and the need to avoid a weak layer in the first floor. The proposed design story shear distribution represents the envelope story shear distribution of the structure, due to the ground motion records used in this study, very well, because it is based on inelastic behavior.

Acknowledgments

The authors are grateful for the financial support received from the National Natural Science Foundation of China (Grant No. 51608441) and Special project of the science research program of the education department of Shaanxi province (Grant No. 17JK0542).

References

AISC341-10 (2010), Seismic Provision for Structure Steel Buildings, American Institute of Steel Construction, Chicago, USA.

Akiyama, H. (1985), *Earthquake-Resistant Limit-State Design for Buildings*, University of Tokyo Press, Tokyo, Japan.

Ashikov, A., Clifton, G.C. and Belev, B. (2016), "Finite element analysis of eccentrically braced frames with a new type of bolted replaceable active link", *New Zealand Society for Earthquake Engineering 2016 Conference*.

Azad, S.K. and Topkaya, C. (2017), "A review of research on steel eccentrically braced frames", *J. Constr. Steel Res.*, **128**(1), 53-73.

Berman, J.W. and Bruneau, M. (2007), "Experimental and analytical investigation of tubular links for eccentrically braced frames", *Eng. Struct.*, **29**(8), 1929-1938.

Bosco, M. and Rossi, P.P. (2009), "Seismic behaviour of eccentrically braced frames", *Eng. Struct.*, **31**(3), 664-674.

Chao, S.H., Goel, S.C. and Lee, S.S. (2007), "A seismic design lateral force distribution based on inelastic state of structures", *Earthq. Spectra*, **23**(3), 547-569.

Daneshmand, A. and Hashemi, B.H. (2012), "Performance of intermediate and long links in eccentrically braced frames", *J. Constr. Steel Res.*, **70**(3), 167-176.

Engelhardt, M.D. and Popov, E.P. (1992), "Experimental performance of long links in eccentrically braced frames", *J. Struct. Eng.*, **118**(11), 3067-3088.

Foutch, D.A. (1989), "Seismic behavior of eccentrically braced steel building", *J. Struct. Eng.*, **115**(8), 1857-1876.

GB50011-2010 (2010), Code for seismic design of buildings, China Architecture Industry Press, Beijing, China. (in Chinese)

Hjelmstad, K.D. and Popov, E.P. (1983), "Cyclic behavior and design of link beams", *J. Struct. Eng.*, **109**(10), 2387-2403.

Hjelmstad, K.D. and Popov, E.P. (1984), "Characteristics of eccentrically braced frames", *J. Struct. Eng.*, **110**(2), 340-353.

Housner, G.W. (1956), "Limit design of structures to resist earthquakes", *Proceedings of the First World Conference on Earthquake Engineering*, Earthquake Engineering Research Institute, Berkeley, CA.

Housner, G.W. (1960), "The plastic failure of frames during earthquakes", *Proceedings of the Second World Conference on Earthquake Engineering*, Internationa Association of Earthquake Engineering ,Tokyo.

Kasai, K. and Popov, E.P. (1986), "General behavior of wf steel shear link beams", *J. Struct. Eng.*, **112**(2), 362-382.

Lee, S.S., Goel, S.C. and Chao, S.H. (2004), "Performance-based design of steel moment frames using target drift and yield mechanism", Ph.D. Dissertation.

Lee, S.S., Goel, S.C. and Stojadinovi, B. (2012), "Toward performance-based seismic design of structures", *Earthq. Spectra*, **15**(3), 435-461.

Lee, S.S., Goel, S.C. and Stojadinovic, B. (1998), "Drift and yield mechanism based seismic design and upgrading of steel moment frames", Ph.D. Dissertation.

Lian, M., Su, M.Z. and Guo, Y. (2015), "Seismic performance of eccentrically braced frames with high strength steel combination", *Steel Compos. Struct.*, **18**(6), 1517-1539.

Liao, W.C. (2010), "Performance-based plastic design of earthquake resistant reinforced concrete moment frames", Ph.D. Dissertation, The University of Michigan, Michigan.

Malley, J.O. and Popov, E.P. (1984), "Shear links in eccentrically

braced frames", *J. Struct. Eng.*, **110**(9), 2275-2295.
Mansour, N., Christopoulos, C. and Tremblay, R. (2011), "Experimental validation of replaceable shear links for eccentrically braced steel frames", *J. Struct. Eng.*, **137**(10), 1141-1152.
Miranda, E. and Bertero, V.V. (1994), "Evaluation of strength reduction factors for earthquake-resistant design", *Earthq. Spectra*, **10**(2), 357-379.
Newmark, N.M. and Hall, W.J. (1982), *Earthquake Spectra and Design*, Earthquake Engineering Research Institute, El Cerrito, CA.
Shen, Y., Christopoulos, C., Mansour, N. and Tremblay, R. (2011), "Seismic design and performance of steel moment-resisting frames with nonlinear replaceable links", *J. Struct. Eng.*, **137**(10), 1107-1117.
Speicher, M.S. and Iii, J.L.H. (2016), "Collapse prevention seismic performance assessment of new eccentrically braced frames using ASCE 41", *Eng. Struct.*, **117**(6), 344-357.
Uang, C.M. and Bertero, V.V. (1988), "Use of energy as a design criterion in earthquake-resistant design", Research Report No. UCB/EERC-88/18, Earthquake Engineering Research Center, University of California, Berkeley, CA.
Wang, F., Su, M.Z., Hong, M., Guo, Y. and Li, S. (2016), "Cyclic behaviour of y-shaped eccentrically braced frames fabricated with high-strength steel composite", *J. Constr. Steel Res.*, **120**(2), 176-187.

CC

Notations

θ_y	yield drift	A_c	area of the column cross section
θ_u	ultimate drift	ε	average strain in columns
θ_{ys}	shear drift	H	structure height
θ_{yf}	bending drift	F	lateral force
h	storey height	Δ_{vert}	vertical axial deformation
a	beam length outside link	Δ_{horiz}	horizontal deformation
e	link length	H_j	the height of level j from the base
L_b	the length of brace	G_n	the weight at the top level
L	the span of the EBFs	H_n	the height of roof level from base
θ	the angle of the brace	T	the fundamental period
ε_{yb}	the strain of brace	F_i	the lateral force at level i
f_{yb}	yield strength of the braces	V	the total design base shear
E	modulus of elasticity	γ	the energy modification factor
σ	average axial stress in columns owing to overturning moment	μ_s	the structural ductility factor
M	overturning moment caused by the lateral loads	R_μ	the ductility reduction factor
f_{yc}	yield strength of the columns	S_v	the design spectral pseudo velocity
γ_R	material partial coefficients	E_e	the elastic components of the energy
θ_p	plastic drift	E_p	the plastic components of the energy
γ_p	plastic rotation of link	ψ	strength reduction factor
β_i	the shear distribution factor at level i	f_y	the yielding strength of links
V_i	the story shear forces at level i	$A_{w,i}$	the web area of ith story link
V_n	the story shear forces at the top (nth) level	V'	one-bay base shear
G_j	the seismic weight at level j	h_1	the bottom story height
ξ	a dimensionless parameter	V_u	ultimate shear capacity of link
ω_i	the vertical force in ith story beams	λ_i	the lateral force distribution coefficient
M_{pc}	the plastic moment of column base	$M_{pb,i}$	the plastic moment of beams with no braces
V_{pr}	plastic shear strength of top story link	$V_{pb,i}$	the corresponding shear force with $M_{pb,i}$
$\beta_i V_{\text{pr}}$	the plastic shear strength of ith story link.	P_{brace}	the axial force of brace
I	moment of inertia of the EBFs		